The Response of Layered Anisotropic Tubes to Centrifugal Loading

H.W. Carpenter[a,*], R.G. Reid[b]

[a]*Necsa SOC Limited, PO Box 582, Pretoria 0001, Republic of South Africa*
[b]*DST/NRF Centre of Excellence in Strong Materials and RP/Composites Facility*
School of Mechanical, Industrial and Aeronautical Engineering
University of the Witwatersrand, Johannesburg
Private Bag 3, Wits, 2050, South Africa

Abstract

The displacement-based elastic solution for layered anisotropic tubes is extended to allow for the presence of centrifugal loading. The additional terms in the stress-strain equations derived in this work are validated by comparing the results obtained using the current solution against those determined using finite element simulation of rotating thin and thick-walled glass fibre reinforced plastic tubes of arbitrary anisotropic lay-up. The solution is presented in such a form that it can be utilised to determine the linear thermo-mechanical behaviour of rotating tubes with anisotropic lay-up, subjected to any combination of internal and external axisymmetric pressure, axial loading, torsional loading, and constant temperature change.

Keywords: Anisotropic tubes, Centrifugal Loading, Elastic Solution

Introduction

In recent years fibre reinforced plastic (FRP) materials have been increasingly utilised because of the excellent strength-to-weight ratio and good corrosion resistance properties that they exhibit. One of the most important structures manufactured from these materials are tubes, which are widely used across many industries and in many different applications. FRP tubes are most widely used in the form of pipes for the transportation of corrosive substances, but they are also becoming frequently used as drive shafts in the automotive and aerospace industries. Depending on the stacking sequence of the plies of which a tube is comprised, the material properties may be transversely isotropic, orthotropic, or even anisotropic. The complex behaviour of such tubes has led to an appreciable body of research which is aimed at describing the elastic behaviour of these structures. Fortunately, due to the cylindrical nature of a tube, its elastic response is well defined, and numerous exact analytical solutions have been

*Corresponding author
Email address: Henry.Carpenter@necsa.co.za (H.W. Carpenter)

developed for FRP tubes under various loading conditions. One of the pioneering researchers in this regard was Lekhnitskii [1], and his work, which is based upon a stress function approach, has formed the basis of many analytical models [2–4] describing the response of composite tubes to different loads, and also for the measurement of residual stresses in cylindrically orthotropic tubes [5–8]. Stroh formalism [9] has also formed a fundamental platform upon which numerous analytical solutions [10–14] for composite tubes have been developed. Significant in these works is the state-space approach first presented by Tarn and Wang [13]. Another of the commonly utilised elastic solutions for the analysis of multi-layered, anisotropic tubes can be referred to as the displacement approach, and is fundamentally based upon, among others, the works of Sherrer [15], Reissner and Tsai [16], Wilson and Orgill [17, 18], Kollár et al. [19], and Kollár and Springer [20]. This solution considers only axisymmetric thermomechanical loading, with the absence of out-of-plane shear forces. Under these circumstances, a generalised plane-strain condition arises, where the axial strain is constant over the wall thickness. This condition was initially realised by Leknitskii [1], and resonates in many subsequent works. The displacement-based elastic solution has been presented in many forms [21–25] and appears to have been first derived by Rousseau et al. [21]. The textbook of Herakovich [23] provides an in-depth derivation of this approach, which has also been extended to take account of material and geometric non-linearities [22], as well as through-thickness thermal variations [25].

None of the works mentioned thus far consider body forces associated with inertial loading. A common source of inertial loads in tubular structures is rotation about the longitudinal axis. Examples of composite tubes subjected, but not limited, to this type of loading are FRP drive shafts, flywheels, and centrifuge rotors. The practical importance of such structures means that there has, of course, been much research [26–35] focussed upon analytically describing the behaviour of rotating non-isotropic tubes. These works are, however, somewhat limited in terms of their application to layered FRP tubes. Firstly, many of these works [26–31] assume a state of plane-strain or plane-stress, and are therefore limited only to cases where these assumptions hold true. For instance, a plane-stress condition may arise should the component under consideration take the form of an annular plate or disc. On the other hand, a plane-strain condition may be assumed if the axial stiffness of a fairly long tube is much larger than the circumferential and radial stiffnesses. In general, however, these conditions seldom exist, and for an axisymmetric loading condition, a state of generalised plane-strain [23] arises. Secondly, most of these works [26–30, 32–34] extend only to cylindrically orthotropic materials, and therefore cannot be utilised to analyse the elastic response of a rotating FRP tube of anisotropic lay-up. The only analytical solutions which address these deficiencies are the state-space approaches of Tarn and Wang [13] and Tarn [35]. Tarn and Wang [13] pointed out that centripetal acceleration gives rise to an axisymmetric state, and can be accounted for by adaptation of the governing equations that they presented. Tarn [35] later presented the state-space solution for rotating anisotropic functionally-graded tubes.

Although the state-space approach can be used to address the problem of centrifugal loads, it requires extensive matrix generation and eigen analysis. The displacement-based elastic solution offers a potentially less complex approach. It merely requires a number of constants, dependant on the number of layers in the tube, to be determined.

These are easily found by considering the loading and the inter-laminar boundary conditions. It appears, however, that the displacement-based elastic solution has not yet been extended to account for the response of layered anisotropic tubes subjected to centripetal acceleration. The purpose of the present work is, therefore, to address this issue, and thereby provide an alternative means by which the behaviour of a rotating tube of this nature can be evaluated.

Theory

The derivation of this displacement-based elastic solution for a layered, anisotropic tube, subjected to centrifugal loading, is based upon the derivation presented in the textbook of Herakovich [23]. Consequently, the equations defining the through-thickness stress and strain distributions of the tube are identical to those presented by Herakovich [23], apart from additional terms which are associated with centripetal acceleration and which arise from the rotation of the tube about its central axis. The present derivation includes the terms associated with axisymmetric axial force, torque, internal and external pressures, as well as thermal effects arising from constant temperature change. Although the primary focus of the current work is on the effects of centrifugal loading only, the complete thermo-mechanical solution to the problem is provided so that the response of any rotating layered anisotropic tube, subjected to any combination of axisymmetric thermo-mechanical loading can be determined.

The laminated composite tube under consideration, comprising N layers, is illustrated in Fig. 1. The tube is assumed to be infinitely long, axisymmetic, and uniformly loaded along its length. The loads under consideration are internal and external pressures, P_I and P_O respectively, as well as axial and torque loads, F_x and T_x, which are associated with the integrals over the wall thickness of the axial stress, and the moment of in-plane shear stress, respectively [23]. The tube is assumed to be rotating about the central axis, x, with a constant angular velocity, Ω. Under the axisymmetric condition, all displacements, strains, and stresses are independent of the circumferential position, θ. Additionally, the radial displacements, w, are also independent of the axial position, x. The general expressions of the axial, u, circumferential, v, and radial, w, displacements of an arbitrary layer k can therefore be described by Eqs. (1) to (3) [23].

$$u^k = u^k(x,r) \tag{1}$$

$$v^k = v^k(x,r) \tag{2}$$

$$w^k = w^k(r) \tag{3}$$

The strain-displacement equations for each layer k within an infinitely long tube uniformly loaded along its length are [23]:

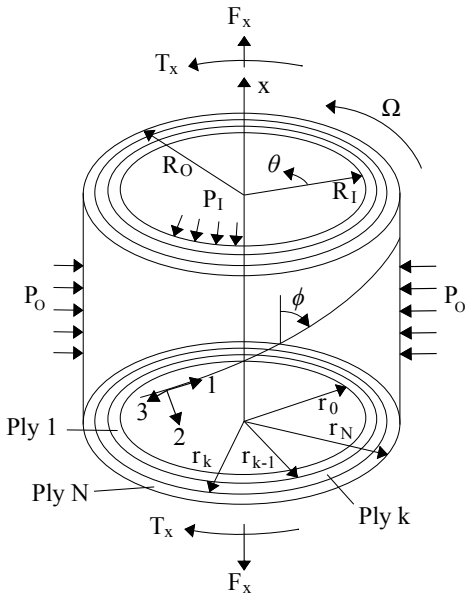

Figure 1: Laminated composite tube

$$\varepsilon_x^k = \frac{\partial u^k}{\partial x} \tag{4}$$

$$\varepsilon_\theta^k = \frac{w^k}{r} \tag{5}$$

$$\varepsilon_r^k = \frac{\partial w^k}{\partial r} \tag{6}$$

$$\gamma_{\theta r}^k = \frac{\partial v^k}{\partial r} - \frac{v^k}{r} \tag{7}$$

$$\gamma_{xr}^k = \frac{\partial u^k}{\partial r} \tag{8}$$

$$\gamma_{x\theta}^k = \frac{\partial v^k}{\partial x} \tag{9}$$

The compatibility equations, associated with axisymmetric displacement continuity are [23]:

$$\frac{d^2\varepsilon_x^k}{dr^2} = 0 \tag{10}$$

$$\frac{1}{r}\frac{d\varepsilon_x^k}{dr} = 0 \tag{11}$$

$$\frac{1}{2}\frac{d}{dr}\left[\frac{1}{r}\frac{d}{dr}\left(r\gamma_{x\theta}^k\right)\right] = 0 \tag{12}$$

Integration of Eqs. (10) and (11) demonstrates that the axial strain within any layer k must be constant. Defining this constant as $\varepsilon_x^{0^k}$, the axial strain within this layer can be written as:

$$\varepsilon_x^k = \varepsilon_x^{0^k} \tag{13}$$

For an orthotropic layer k, the thermo-elastic constitutive equations in the principal material directions $(1,2,3)$ are [23]:

$$\begin{bmatrix} \sigma_1^k \\ \sigma_2^k \\ \sigma_3^k \\ \tau_{23}^k \\ \tau_{31}^k \\ \tau_{12}^k \end{bmatrix} = \begin{bmatrix} C_{11}^k & C_{12}^k & C_{13}^k & 0 & 0 & 0 \\ C_{12}^k & C_{22}^k & C_{23}^k & 0 & 0 & 0 \\ C_{13}^k & C_{23}^k & C_{33}^k & 0 & 0 & 0 \\ 0 & 0 & 0 & C_{44}^k & 0 & 0 \\ 0 & 0 & 0 & 0 & C_{55}^k & 0 \\ 0 & 0 & 0 & 0 & 0 & C_{66}^k \end{bmatrix} \begin{bmatrix} \varepsilon_1^k - \varepsilon_1^{k^T} \\ \varepsilon_2 - \varepsilon_2^{k^T} \\ \varepsilon_3 - \varepsilon_3^{k^T} \\ \gamma_{23}^k \\ \gamma_{31}^k \\ \gamma_{12}^k \end{bmatrix} \tag{14}$$

For a fibre orientation, ϕ, measured from the axial direction, the thermo-elastic constitutive equations for this layer, in the cylindrical coordinate system (x,θ,r), can be transformed to [23]:

$$\begin{bmatrix} \sigma_x^k \\ \sigma_\theta^k \\ \sigma_r^k \\ \tau_{\theta r}^k \\ \tau_{xr}^k \\ \tau_{x\theta}^k \end{bmatrix} = \begin{bmatrix} \bar{C}_{11}^k & \bar{C}_{12}^k & \bar{C}_{13}^k & 0 & 0 & \bar{C}_{16}^k \\ \bar{C}_{12}^k & \bar{C}_{22}^k & \bar{C}_{23}^k & 0 & 0 & \bar{C}_{26}^k \\ \bar{C}_{13}^k & \bar{C}_{23}^k & \bar{C}_{33}^k & 0 & 0 & \bar{C}_{36}^k \\ 0 & 0 & 0 & \bar{C}_{44}^k & \bar{C}_{45}^k & 0 \\ 0 & 0 & 0 & \bar{C}_{45}^k & \bar{C}_{55}^k & 0 \\ \bar{C}_{16}^k & \bar{C}_{26}^k & \bar{C}_{36}^k & 0 & 0 & \bar{C}_{66}^k \end{bmatrix} \begin{bmatrix} \varepsilon_x^k - \varepsilon_x^{k^T} \\ \varepsilon_\theta^k - \varepsilon_\theta^{k^T} \\ \varepsilon_r^k - \varepsilon_r^{k^T} \\ \gamma_{\theta r}^k \\ \gamma_{xr}^k \\ \gamma_{x\theta}^k - \gamma_{x\theta}^{k^T} \end{bmatrix} \tag{15}$$

The transformed stiffness matrix, $\bar{C}$, is obtained [23] through the transformation equation:

$$[\bar{C}] = [T_1]^{-1}[C][T_2] \tag{16}$$

The transformation matrices [23], T_1 and T_2, are defined by Eqs. (17) and (18):

$$T_1 = \begin{bmatrix} m^2 & n^2 & 0 & 0 & 0 & 2mn \\ n^2 & m^2 & 0 & 0 & 0 & -2mn \\ 0 & 0 & 1 & 0 & 0 & 0 \\ 0 & 0 & 0 & m & -n & 0 \\ 0 & 0 & 0 & n & m & 0 \\ -mn & mn & 0 & 0 & 0 & m^2-n^2 \end{bmatrix} \tag{17}$$

$$T_2 = \begin{bmatrix} m^2 & n^2 & 0 & 0 & 0 & mn \\ n^2 & m^2 & 0 & 0 & 0 & -mn \\ 0 & 0 & 1 & 0 & 0 & 0 \\ 0 & 0 & 0 & m & -n & 0 \\ 0 & 0 & 0 & n & m & 0 \\ -2mn & 2mn & 0 & 0 & 0 & m^2-n^2 \end{bmatrix} \tag{18}$$

where $m = \cos\phi$ and $n = \sin\phi$.

For any cylindrical body, equilibrium in the radial, circumferential, and axial directions, respectively, requires that [1, 23]:

$$\frac{\partial \sigma_r}{\partial r} + \frac{1}{r}(\sigma_r - \sigma_\theta) + \frac{1}{r}\frac{\partial \tau_{\theta r}}{\partial \theta} + \frac{\partial \tau_{xr}}{\partial x} + B_r = 0 \tag{19}$$

$$\frac{\partial \tau_{\theta r}}{\partial r} + \frac{1}{r}\frac{\partial \sigma_\theta}{\partial \theta} + \frac{\partial \tau_{x\theta}}{\partial x} + \frac{2}{r}\tau_{\theta r} + B_\theta = 0 \tag{20}$$

$$\frac{\partial \tau_{xr}}{\partial r} + \frac{1}{r}\frac{\partial \tau_{x\theta}}{\partial \theta} + \frac{\partial \sigma_x}{\partial x} + \frac{1}{r}\tau_{xr} + B_x = 0 \tag{21}$$

where B_r, B_θ, and B_x are the body forces in each of these directions, respectively. Under the axisymmetric condition, in regions free from edge effects, the stresses that develop within a tube are independent of x and θ. Additionally, the body forces that arise due to rotation of the tube about its central axis act only in the radial direction. As a consequence, Eqs. (19) to (21) can be simplified, and the equilibrium conditions within an arbitrary layer k of a rotating laminated anisotropic tube can therefore be described by Eqs. (22) to (24) [23, 36].

$$\frac{d\sigma_r^k}{dr} + \frac{\sigma_r^k - \sigma_\theta^k}{r} + \rho^k \Omega^2 r = 0 \tag{22}$$

$$\frac{d\tau_{\theta r}^k}{dr} + \frac{2\tau_{\theta r}^k}{r} = 0 \tag{23}$$

$$\frac{d\tau_{xr}^k}{dr} + \frac{\tau_{xr}^k}{r} = 0 \tag{24}$$

The term ρ^k in Eq. (22) is the density of the material from which layer k is composed. It is assumed that the layer is homogeneous, and therefore ρ^k is constant. Integration of Eqs. (23) and (24), respectively, gives the through thickness shear stresses, $\tau_{\theta r}$ and τ_{xr}, of layer k in the form of Eqs. (25) and (26).

$$\tau_{\theta r}^k = \frac{H^k}{r^2} \tag{25}$$

$$\tau_{xr}^k = \frac{I^k}{r} \tag{26}$$

Since no shear stresses in these two senses are applied, the constants H^k and I^k of each layer must be zero [23]. This result can be obtained by considering the inner or outer surfaces of the tube. At these surfaces, the absence of any applied stresses $\tau_{\theta r}$ and τ_{xr}, requires that the constants H^1 and I^1, associated with the inner layer, and the constants H^N and I^N, associated with the outermost layer, be zero. Additionally, traction continuity between all adjacent layers requires that the through-thickness shear stresses of Eqs. (25) and (26) be continuous from layer to layer, which leads to the result that all H^k and I^k constants must be zero. Therefore, the shear stresses $\tau_{\theta r}^k$ and τ_{xr}^k must be zero through the entire wall thickness of the tube. Consequently, by Eq. (15), the through-thickness shear strains, $\gamma_{\theta r}^k$ and γ_{xr}^k, must also be zero for all layers. It must be stressed that this condition is only valid in regions free of edge effects, and for tubes under the prescribed axisymmetric loading conditions.

Integrating the compatibility condition of Eq. (12), the in-plane shear strain $\gamma_{x\theta}^k$ of layer k can be written in the form:

$$\gamma_{x\theta}^k = K_1^k r + \frac{K_2^k}{r} \tag{27}$$

where K_1^k and K_2^k are constants of integration. Combining Eq. (27) with Eq. (9) gives the circumferential displacement as:

$$v^k = \left[K_1^k r + \frac{K_2^k}{r} \right] x + g^k(r) \tag{28}$$

where $g^k(r)$ is an arbitrary function dependant on r only. Substituting Eq. (28) into Eq. (7), the through-thickness shear strain $\gamma_{\theta r}$ can be described by Eq. (29).

$$\gamma_{\theta r}^k = \frac{d}{dr} g^k(r) - \frac{2K_2^k x}{r^2} - \frac{g^k(r)}{r} \tag{29}$$

It has been demonstrated that the through-thickness shear strain, $\gamma_{\theta r}$, is zero through the wall thickness of any layered tube in regions free of edge effects, therefore:

$$\gamma_{\theta r}^k = 0 = \frac{d}{dr} g^k(r) - \frac{2K_2^k x}{r^2} - \frac{g^k(r)}{r} \tag{30}$$

Differentiating Eq. (30) with respect to x, it can be shown that the constant K_2^k is also zero. Substituting this result into Eq. (27) demonstrates that the angle of twist per unit length must be constant through the thickness of layer k:

$$\gamma_{x\theta}^k = K_1^k r \tag{31}$$

Finally, displacement continuity conditions require that the circumferential displacements, v^k, be continuous across all layers. As a consequence, the in-plane shear strain must be continuous across all layers, and therefore the angle of twist per unit length of all layers is identical [23]:

$$K_1^k = \gamma^0 \qquad (k = 1, ..., N) \tag{32}$$

where γ^0 is the angle of twist per unit length of the tube. This is a condition often referred to as the state of generalised torsion, and was first realised by Lekhnitskii [1]. The axial displacements, u^k, must also be continuous across all layers and consequently the axial strain must be continuous across all layers. Since, by Eq. (13), the axial strain within each layer k is constant, the axial strain across all layers must also be constant. This is the state of generalised plane-strain. The axial strain within any layer k can therefore be written as [23]:

$$\varepsilon_x^{0^k} = \varepsilon_x^0 \qquad (k = 1, ..., N) \tag{33}$$

where ε_x^0 is the constant axial strain across the wall thickness of the tube. Combining the results of Eqs. (32) and (33) with Eqs. (31) and (13), and the strain-displacement relationships of Eqs. (5) and (6), with the constitutive relationships of Eq. (15), and substituting of these into the equilibrium condition of Eq. (22) gives a second order ODE for the radial displacement w in the form:

$$\frac{d^2w^k}{dr^2}+\frac{1}{r}\frac{dw^k}{dr}-\frac{\bar{C}^k_{22}}{\bar{C}^k_{33}}\frac{w^k}{r^2}=\frac{1}{\bar{C}^k_{33}}\left[\frac{(\bar{C}^k_{12}-\bar{C}^k_{13})\varepsilon^0_x+\Upsilon^k}{r}+(\bar{C}^k_{26}-2\bar{C}^k_{36})\gamma^0-\rho^k\Omega^2 r\right] \tag{34}$$

where [23]:

$$\Upsilon^k=(\bar{C}^k_{13}-\bar{C}^k_{12})\varepsilon_x^{k^T}+(\bar{C}^k_{23}-\bar{C}^k_{22})\varepsilon_\theta^{k^T}+(\bar{C}^k_{33}-\bar{C}^k_{32})\varepsilon_r^{k^T}+(\bar{C}^k_{63}-\bar{C}^k_{62})\gamma_{x\theta}^{k^T} \tag{35}$$

Eq. (35) can be simplified to:

$$\Upsilon^k=\sum(\bar{C}^k_{i3}-\bar{C}^k_{i2})\varepsilon_i^{k^T}\qquad(i=1,2,3,6) \tag{36}$$

For a constant temperature change, ΔT, the thermal strains of Eq. (36) can be written in terms of the coefficients of thermal expansion [23]:

$$\varepsilon_i^{k^T}=\alpha_i^k\Delta T \tag{37}$$

where the coefficients of thermal expansion are

$$\alpha^k=\begin{bmatrix}\alpha_x^k\\ \alpha_\theta^k\\ \alpha_r^k\\ 0\\ 0\\ \alpha_{x\theta}^k\end{bmatrix} \tag{38}$$

Defining

$$\tilde{\Upsilon}^k=\sum(\bar{C}^k_{i3}-\bar{C}^k_{i2})\alpha_i^k\qquad(i=1,2,3,6) \tag{39}$$

the thermal term Υ^k can be written as

$$\Upsilon^k=\tilde{\Upsilon}^k\Delta T \tag{40}$$

Substituting this result into Eq. (34), the ODE of the radial displacement takes the form

$$\frac{d^2w^k}{dr^2}+\frac{1}{r}\frac{dw^k}{dr}-\frac{\bar{C}^k_{22}}{\bar{C}^k_{33}}\frac{w^k}{r^2}=\frac{1}{\bar{C}^k_{33}}\left[\frac{(\bar{C}^k_{12}-\bar{C}^k_{13})\varepsilon^0_x+\tilde{\Upsilon}^k\Delta T}{r}+(\bar{C}^k_{26}-2\bar{C}^k_{36})\gamma^0-\rho^k\Omega^2 r\right] \tag{41}$$

The radial displacement w^k can be found by solving Eq. (41). The solution to this ODE is presented in Eq. (42).

$$\begin{aligned} w^k(r) = A_1^k r^{\lambda^k} + A_2^k r^{-\lambda^k} + \left(\frac{\bar{C}_{12}^k - \bar{C}_{13}}{\bar{C}_{33} - \bar{C}_{22}^k}\right)\varepsilon_x^0 r + \left(\frac{\bar{C}_{26}^k - 2\bar{C}_{36}^k}{4\bar{C}_{33}^k - \bar{C}_{22}^k}\right)\gamma^0 r^2 \\ + \left(\frac{\tilde{\Upsilon}^k}{\bar{C}_{33}^k - \bar{C}_{22}^k}\right) r\Delta T - \left(\frac{\rho^k}{9\bar{C}_{33}^k - \bar{C}_{22}^k}\right)\Omega^2 r^3 \end{aligned} \tag{42}$$

where

$$\lambda^k = \sqrt{\frac{\bar{C}_{22}^k}{\bar{C}_{33}}} \tag{43}$$

and A_1^k and A_2^k are constants of the general solution of the ODE. Defining the terms Γ^k, β^k, Ψ^k, and ξ^k as

$$\Gamma^k = \frac{\bar{C}_{12}^k - \bar{C}_{13}^k}{\bar{C}_{33}^k - \bar{C}_{22}^k} \tag{44}$$

$$\beta^k = \frac{\bar{C}_{26}^k - 2\bar{C}_{36}^k}{4\bar{C}_{33}^k - \bar{C}_{22}^k} \tag{45}$$

$$\Psi^k = \frac{\tilde{\Upsilon}^k}{\bar{C}_{33}^k - \bar{C}_{22}^k} \tag{46}$$

$$\xi^k = \frac{\rho^k}{9\bar{C}_{33}^k - \bar{C}_{22}^k} \tag{47}$$

respectively, the radial displacement at any particular radial position r, within layer k, can be simplified to

$$w^k(r) = A_1^k r^{\lambda^k} + A_2^k r^{-\lambda^k} + \Gamma^k \varepsilon_x^0 r + \beta^k \gamma^0 r^2 + \Psi^k r\Delta T - \xi^k \Omega^2 r^3 \tag{48}$$

Combining Eqs. (32) and (33) with Eqs. (31) and (13), and substituting these into Eqs. (4) and (9), and ignoring the constants of integration associated with rigid body motion, the remaining axial and circumferential displacements at the radial position r are [23]

$$u^k(x,r) = \varepsilon_x^0 x \tag{49}$$

$$v^k(x,r) = \gamma^0 xr \tag{50}$$

Substituting Eqs. (48) to (50) into Eqs. (4) to (9), the generalised strains at the radial position r, within layer k of the laminated tube, can be expressed as

$$\varepsilon_x^k(r) = \varepsilon_x^0 \tag{51}$$

$$\begin{aligned}\varepsilon_\theta^k(r) = {} & A_1^k r^{\lambda^k - 1} + A_2^k r^{-\lambda^k - 1} + \Gamma^k \varepsilon_x^0 + \beta^k \gamma^0 r \\ & + \Psi^k \Delta T - \xi^k \Omega^2 r^2\end{aligned} \tag{52}$$

$$\begin{aligned}\varepsilon_r^k(r) = {} & \lambda^k A_1^k r^{\lambda^k - 1} - \lambda^k A_2^k r^{-\lambda^k - 1} + \Gamma^k \varepsilon_x^0 + 2\beta^k \gamma^0 r \\ & + \Psi^k \Delta T - 3\xi^k \Omega^2 r^2\end{aligned} \tag{53}$$

$$\gamma_{x\theta}^k(r) = \gamma^0 r \tag{54}$$

$$\gamma_{\theta r}^k(r) = 0 \tag{55}$$

$$\gamma_{xr}^k(r) = 0 \tag{56}$$

The stresses can be determined directly from the constitutive relationships of Eq. (15) and the generalised strains presented in Eqs. (51) to (54). The resulting stresses within layer k, at the radial position r, are presented in Eqs. (57) to (62).

$$\sigma_x^k(r) = \left[\bar{C}_{11}^k + \left(\bar{C}_{13}^k + \bar{C}_{12}^k\right)\Gamma^k\right]\varepsilon_x^0 + \left[\left(\bar{C}_{12}^k + 2\bar{C}_{13}^k\right)\beta^k + \bar{C}_{16}^k\right]\gamma^0 r + \left[\left(\bar{C}_{12}^k + \bar{C}_{13}^k\right)\Psi^k - \bar{C}_{i1}^k\alpha_i^k\right]\Delta T + \left(\bar{C}_{12}^k + \lambda^k\bar{C}_{13}^k\right)A_1^k r^{\lambda^k-1} + \left(\bar{C}_{12}^k - \lambda^k\bar{C}_{13}^k\right)A_2^k r^{-\lambda^k-1} - \left(\bar{C}_{12}^k + 3\bar{C}_{13}^k\right)\xi^k\Omega^2 r^2 \quad (i \text{ sum},\ i = 1,2,3,6) \tag{57}$$

$$\sigma_\theta^k(r) = \left[\bar{C}_{12}^k + \left(\bar{C}_{22}^k + \bar{C}_{23}^k\right)\Gamma^k\right]\varepsilon_x^0 + \left[\left(\bar{C}_{22}^k + 2\bar{C}_{23}^k\right)\beta^k + \bar{C}_{26}^k\right]\gamma^0 r + \left[\left(\bar{C}_{22}^k + \bar{C}_{23}^k\right)\Psi^k - \bar{C}_{i2}^k\alpha_i^k\right]\Delta T + \left(\bar{C}_{22}^k + \lambda^k\bar{C}_{23}^k\right)A_1^k r^{\lambda^k-1} + \left(\bar{C}_{22}^k - \lambda^k\bar{C}_{23}^k\right)A_2^k r^{-\lambda^k-1} - \left(\bar{C}_{22}^k + 3\bar{C}_{23}^k\right)\xi^k\Omega^2 r^2 \quad (i \text{ sum},\ i = 1,2,3,6) \tag{58}$$

$$\sigma_r^k(r) = \left[\bar{C}_{13}^k + \left(\bar{C}_{23}^k + \bar{C}_{33}^k\right)\Gamma^k\right]\varepsilon_x^0 + \left[\left(\bar{C}_{23}^k + 2\bar{C}_{33}^k\right)\beta^k + \bar{C}_{36}^k\right]\gamma^0 r + \left[\left(\bar{C}_{23}^k + \bar{C}_{33}^k\right)\Psi^k - \bar{C}_{i3}^k\alpha_i^k\right]\Delta T + \left(\bar{C}_{23}^k + \lambda^k\bar{C}_{33}^k\right)A_1^k r^{\lambda^k-1} + \left(\bar{C}_{23}^k - \lambda^k\bar{C}_{33}^k\right)A_2^k r^{-\lambda^k-1} - \left(\bar{C}_{23}^k + 3\bar{C}_{33}^k\right)\xi^k\Omega^2 r^2 \quad (i \text{ sum},\ i = 1,2,3,6) \tag{59}$$

$$\tau_{x\theta}^k(r) = \left[\bar{C}_{16}^k + \left(\bar{C}_{26}^k + \bar{C}_{36}^k\right)\Gamma^k\right]\varepsilon_x^0 + \left[\left(\bar{C}_{26}^k + 2\bar{C}_{36}^k\right)\beta^k + \bar{C}_{66}^k\right]\gamma^0 r + \left[\left(\bar{C}_{26}^k + \bar{C}_{36}^k\right)\Psi^k - \bar{C}_{i6}^k\alpha_i^k\right]\Delta T + \left(\bar{C}_{26}^k + \lambda^k\bar{C}_{36}^k\right)A_1^k r^{\lambda^k-1} + \left(\bar{C}_{26}^k - \lambda^k\bar{C}_{36}^k\right)A_2^k r^{-\lambda^k-1} - \left(\bar{C}_{26}^k + 3\bar{C}_{36}^k\right)\xi^k\Omega^2 r^2 \quad (i \text{ sum},\ i = 1,2,3,6) \tag{60}$$

$$\tau_{\theta r}^k(r) = 0 \tag{61}$$

$$\tau_{xr}^k(r) = 0 \tag{62}$$

To determine the stress and strain distributions through the thickness of a laminated composite tube, the constants ε_x^0, γ^0, A_1^k, and A_2^k need to be found. For a tube comprising N layers, this translates to $2(N+1)$ constants, and these can be determined from the specific loading and boundary conditions that exist. As has been mentioned, the axial force applied at the ends of the tube, F_x, is exactly the integral of the axial stress that

exists over the tube cross section [23]. Integrating Eq. (57) in this manner allows the axial force to be expressed in terms of ε_x^0, γ^0, A_1^k, and A_2^k:

$$\begin{aligned}
F_x &= \int_{R_I}^{R_O} 2\pi\sigma_x(r) r dr \\
&= 2\pi \sum_{k=1}^{N} \int_{r_{k-1}}^{r_k} \sigma_x^k(r) r dr \\
&= 2\pi \sum_{k=1}^{N} \left\{ \left[\left\{ \bar{C}_{11}^k + \left(\bar{C}_{13}^k + \bar{C}_{12}^k \right) \right\} \varepsilon_x^0 + \left\{ \left(\bar{C}_{12}^k + \bar{C}_{13}^k \right) \Psi^k - \bar{C}_{i1}^k \alpha_i^k \right\} \Delta T \right] \right. \\
&\quad \left(\frac{r_k^2 - r_{k-1}^2}{2} \right) + \left[\bar{C}_{16}^k + \left(\bar{C}_{12}^k + 2\bar{C}_{13}^k \right) \beta^k \right] \gamma^0 \left(\frac{r_k^3 - r_{k-1}^3}{3} \right) + \frac{\bar{C}_{12}^k + \lambda^k \bar{C}_{13}^k}{\lambda^k + 1} \\
&\quad A_1^k \left(r_k^{\lambda^k + 1} - r_{k-1}^{\lambda^k + 1} \right) + \frac{\bar{C}_{12}^k - \lambda^k \bar{C}_{13}^k}{-\lambda^k + 1} A_2^k \left(r_k^{\lambda^k + 1} - r_{k-1}^{-\lambda^k + 1} \right) - \left[\bar{C}_{12}^k + 3\bar{C}_{13}^k \right] \\
&\quad \left. \xi^k \Omega^2 \left(\frac{r_k^4 - r_{k-1}^4}{4} \right) \right\} \quad (i \text{ sum, } i = 1,2,3,6)
\end{aligned} \tag{63}$$

It is must be emphasised that in Eq. (63), the radial position r_k refers to the interface between layers k and $k+1$, respectively. This is also indicated in Fig. 1. Using this notation, it is clear that the radial position $r_0 = R_I$ corresponds to the inner surface of the tube. Similarly, the radial position $r_N = R_O$ corresponds to the outer surface of the tube. The torque carried by the tube, T_x, is the integral of the moment of the in-plane shear stresses about the centreline of the tube [23]. Integrating Eq. (60) in this manner gives:

$$\begin{aligned}
T_x &= 2\pi \sum_{k=1}^{N} \left\{ \left[\left\{ \bar{C}_{16}^k + \left(\bar{C}_{26}^k + \bar{C}_{36}^k \right) \right\} \varepsilon_x^0 + \left\{ \left(\bar{C}_{26}^k + \bar{C}_{36}^k \right) \Psi^k - \bar{C}_{i6}^k \alpha_i^k \right\} \Delta T \right] \right. \\
&\quad \left(\frac{r_k^3 - r_{k-1}^3}{3} \right) + \left[\bar{C}_{66}^k + \left(\bar{C}_{26}^k + 2\bar{C}_{36}^k \right) \beta^k \right] \gamma^0 \left(\frac{r_k^4 - r_{k-1}^4}{4} \right) + \frac{\bar{C}_{26}^k + \lambda^k \bar{C}_{36}^k}{\lambda^k + 2} \\
&\quad A_1^k \left(r_k^{\lambda^k + 2} - r_{k-1}^{\lambda^k + 2} \right) + \frac{\bar{C}_{26}^k - \lambda^k \bar{C}_{36}^k}{-\lambda^k + 2} A_2^k \left(r_k^{\lambda^k + 2} - r_{k-1}^{-\lambda^k + 2} \right) - \left[\bar{C}_{26}^k + 3\bar{C}_{36}^k \right] \\
&\quad \left. \xi^k \Omega^2 \left(\frac{r_k^5 - r_{k-1}^5}{5} \right) \right\} \quad (i \text{ sum, } i = 1,2,3,6)
\end{aligned} \tag{64}$$

In addition to the boundary conditions associated with the axial and torque loads, traction continuity requires that the radial stress, $\sigma_r(r)$, at the inner and outer surfaces of the tube be equal and opposite to the applied internal and external pressures, P_I and P_O, respectively [23]. These boundary conditions are presented in the form of Eqs. (65) and (66).

$$\sigma_r^1(r_0) = -P_I \tag{65}$$

$$\sigma_r^N(r_N) = -P_O \tag{66}$$

For a tube comprising only a single layer, $N = 1$, the boundary conditions of Eqs. (63) to (66) can be solved simultaneously to determine the required constants ε_x^0, γ^0, A_1^1, and A_2^1. Once obtained, these constants can be substituted into Eqs. (57) to (60), allowing the through-thickness stresses within the tube to be determined. Should the tube comprise N layers, there are $2(N-1)$ additional A_1 and A_2 constants that need to be found. These are determined by invoking the boundary conditions that exist at each layer interface. Traction continuity requires that the radial stress, $\sigma_r(r)$, be continuous across each layer interface. Additionally, displacement continuity requires that the radial displacements, $w(r)$, be continuous at each interface. These boundary conditions are presented in the form of Eqs. (67) and (68) [23]. It should be noted that the requirement for continuity of the axial and circumferential displacements, $u(x,r)$ and $v(x,r)$, across each ply interface have already been taken into account. The consequence of these continuity requirements are the generalised torque and generalised strain conditions of Eqs. (32) and (33), respectively.

$$\sigma_r^k(r_k) = \sigma_r^{k+1}(r_k) \quad \text{(interface at } r_k,\ k = 1,.....,N-1) \tag{67}$$

$$w^k(r_k) = w^{k+1}(r_k) \quad \text{(interface at } r_k,\ k = 1,.....,N-1) \tag{68}$$

Simultaneously solving Eq. (63) to (66), along with the $2(N-1)$ boundary conditions of Eqs. (67) and (68) allows the constants ε_x^0, γ^0, and the A_1^k and A_2^k constants associated with each layer to be determined. Once these constants are known, the through-thickness stress state can be calculated using Eqs. (57) to (60).

Results and discussion

The derivation presented in the previous section extends the displacement-based elastic solution for long, layered, anisotropic tubes to include the body forces arising from centrifugal loading. This loading results only in additional terms in the equations presented by Herakovich [23], and therefore only these terms need to be validated. The existing terms of these equations require no such validation as they are already well established. A comparison of results obtained using the current solution with those of finite element (FE) solutions for thin and thick-walled rotating glass fibre reinforced plastic (GFRP) tubes is presented. It is demonstrated that, for both of the cases considered, the analytical and FE solutions are indistinguishable from one another, therefore validating the current extension of the analytical solution.

The current solution can be applied to tubes of anisotropic lay-up, and so this case is considered for validation purposes for both the thin and thick-walled conditions. For the FE simulation, the coupling between the normal and shear stress components of an anisotropic material requires that such a tube be modelled in three dimensions. To minimise the number of elements required for these models, the outer radius (R_O) of both tubes was kept relatively small, and set to a value of 15 mm. The tubes each comprise four layers, and share the same ply lay-up. The lay-up, starting from the inner surface, was arbitrarily chosen to be [+20°/-45°/+80°/-30°]. The thickness of the layers of the thin-walled tube were set to 0.25 mm, while those of the thick-walled tube were set to 2.5 mm, resulting in thickness to outer radius (t/R_O) ratios of 2/30 and 2/3, respectively. The tubes were assumed to rotate with an angular velocity of 10^5 RPM to ensure that the magnitude of the stresses arising from the centripetal acceleration were significant.

The Patran/Nastran FE software package was utilised to simulate the rotating GFRP tubes. These were both modelled as a wedge cut from a thin annular disc with the appropriate boundary conditions applied to all surfaces except the inner and outer radii. Each wedge subtended an angle of 0.5° and had a thickness of 0.06 mm. Each layer of GFRP was meshed with 8-noded CHEXA elements [37] of global edge length 0.02 mm. For the thin-walled tube, this resulted in 3 elements in the axial direction, 13 elements through the thickness of each layer and 6 elements in the circumferential direction of all four layers, respectively. For the thick-walled tube, the thickness of each layer comprised 130 elements, while the number of elements in the axial and circumferential directions were the same as that of the thin-walled tube. A single face of the wedge, normal to the axis of rotation, was constrained such that it could not move in either the axial direction (x) or rotate about the x-axis. All of the nodes associated with opposite "free" face of the disc were constrained to move with constant axial displacement and constant angle of twist about the x-axis. This enforces the elastic requirement of constant axial strain, ε_x^0, and constant twist per unit length, γ^0, through the wall thickness of the tube, and was done using a multi-point constraint (MPC). The MPC was defined using rigid body elements (RBE), in particular RBE2 elements [37]. The nodes, corresponding to the two faces aligned normal to the circumferential (θ) direction, were constrained using a cyclic-symmetric constraint, which is also an MPC. The three-dimensional material properties of each ply were found using the GFRP material properties, presented in Table 1, and applying the appropriate transformation, dependant on the fibre orientation [23]. The inertial load, associated with the constant

Table 1: GFRP material properties

Longitudinal modulus, E_1 (MPa)	40887
Transverse modulus, $E_2 = E_3$ (MPa)	7905
Shear modulus, $G_{12} = G_{13}$ (MPa)	2437
Shear modulus, G_{23} (MPa)	2855
Poissons ratio, $\nu_{12} = \nu_{13}$	0.298
Poissons ratio, ν_{23}	0.384
Density, ρ (kg/m^3)	1940

angular velocity of 10^5 RPM, was then applied to the entire geometry and a linear

analysis performed.

The through-thickness hoop stress distributions, obtained for both the thin and thick-walled GFRP tubes using the current analytical method and FE simulation, are illustrated in Fig. 2. The through-thickness radial positions are normalised such that the inner surfaces of the tubes correspond to -1, and the outer surfaces correspond to 1. For both tube configurations, the results of the analytical and FE solutions are indistinguishable from one another. The FE solution, therefore, validates the extension of the analytical method presented in this work. As is expected, the hoop stresses are tensile over the entire wall thickness of the tubes, and are discontinuous across each ply interface. For both cases, the maximum stress occurs within the layer wound at $+80°$. This is again expected, since the wind angle of this layer is significantly larger than that of the other plies, and it therefore has the highest circumferential stiffness. The maximum hoop stress within the thin-walled tube, with a value of about 110 MPa, is more than double the maximum hoop stress which arises in the thick-walled tube, which is only around 50 MPa. This is a somewhat unexpected result, and can be explained by considering the geometric properties of each configuration. Although both tubes share the

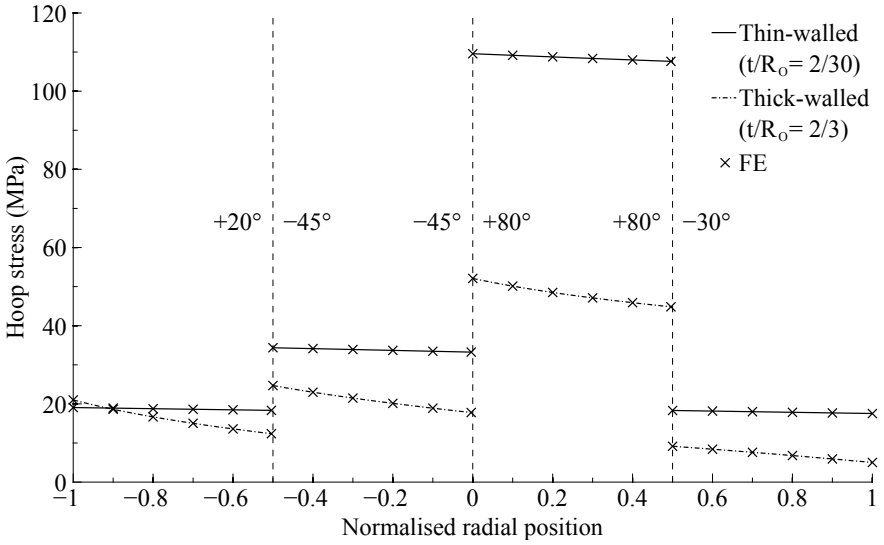

Figure 2: Hoop stress distributions for thin and thick-walled 4 layer anisotropic GFRP tubes

same lay-up and outer radius, the inner radius of the thin-walled tube is significantly larger than that of the thick-walled tube. Consequently, the centrifugal load per unit thickness acting on the plies of the thin-walled tube, particularly those wound at $+20°$, $-45°$, and $+80°$, is considerably larger than that acting on the plies of the thick-walled tube wound with the same fibre orientations. Since the centrifugal loads within these plies are larger for the thin-walled tube, the hoop stresses that develop must also be larger. Another behaviour worth noting is that the hoop stress in each layer tends to decrease with increasing radius. This is most apparent in the thick-walled tube. As a

consequence of this, the hoop stress in the outer ply of -30° orientation is lower than that of the inner ply of $+20^\circ$ orientation despite its higher circumferential stiffness. Even though the hoop stresses in the thin-walled tube are generally higher than those in the thick-walled tube, this is not the case at the inner surface. Here, the hoop stress of the thick-walled tube is larger than that of the thin-walled tube. This behaviour arises because the general trend of increasing hoop stress, as the radius decreases, offsets the effects of the decreasing centrifugal load per unit thickness.

The corresponding radial stresses of both the thin and thick-walled configurations, determined using the current method and FE approach, are illustrated in Fig. 3. As with the hoop stress distributions, the radial stress solutions of both methods are indistinguishable from one another, therefore validating the current extension of the elastic solution. As required, the radial stresses tend to zero at the inner and outer surfaces of both tubes and are continuous across each ply interface. For the thin-walled configuration, the radial stress is nearly linear across each layer, and decreases from zero at the inner surface to a minimum compressive value of around -0.6 MPa at the interface between the plies wound at -45° and $+80^\circ$. The stress increases through the $+80^\circ$ ply to a maximum value of about 0.5 MPa at the interface with the outer -30° ply before decreasing to zero at the outer surface. This behaviour can be explained by recognising that the $+80^\circ$ ply is very stiff in the circumferential direction and tends to support the outwards radial displacement of the other plies. The plies inside this layer apply a compressive load as their radial displacement is constrained whereas the ply outside the $+80^\circ$ layer applies a tensile load as a consequence of this constraint. The radial stress distribution that arises within the thick-walled tube is quite different from that of the thin-walled tube, and is a bit unexpected. Except for the stress within the outer ply of -30° wind angle, the radial stresses within this tube are non-linear. In contrast to those which arise within the thin-walled tube, the radial stresses within the thick-walled tube are tensile across the entire wall thickness, and the magnitude of these stresses is significantly larger than that obtained for the thin-walled configuration. The difference in behaviour can be explained by considering that the radial displacement of the thick-walled tube is not constrained by the $+80^\circ$ ply in the same manner as for the thin-walled tube. In this case there is a substantial variation in the centrifugal load, and also in the geometric support provided by the curved geometry, across the wall thickness. As a consequence, each of the inner plies largely carries its own centrifugal load. The inherently tensile nature of the radial stresses therefore becomes apparent in the plies inside the $+80^\circ$ ply. The relative thickness of each ply allows the non-linear nature of the stresses to be observed. Even though each ply carries a significant part of its own centrifugal load there is some transfer of the centrifugal load between the plies local to the regions of each interface. This is deduced by considering the slight decrease in the radial stress within the ply of $+20^\circ$ wind angle as the interface between this ply, and that wound with an angle of -45°, is approached. In this region, the centrifugal load of both plies is similar, and since the -45° has a higher circumferential stiffness than the $+20^\circ$ ply, it somewhat constrains the radial displacement of the $+20^\circ$ ply thereby carrying a larger portion of the circumferential load in this region. The consequence of this is a decrease in the radial stress of the $+20^\circ$ ply local to the ply interface. Similar behaviour can be seen between the plies of -45° and $+80^\circ$ wind angle. The radial stress within the ply of $+80^\circ$ wind angle does not decrease towards

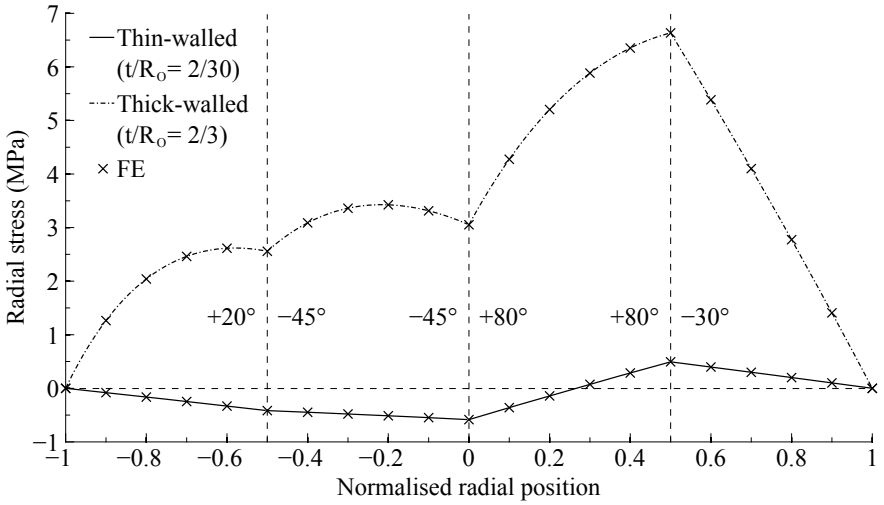

Figure 3: Radial stress distributions for thin and thick-walled 4 layer anisotropic GFRP tubes

its outer surface but instead increases rapidly from a value of roughly 3 MPa to a maximum of more than 6.5 MPa at the interface with the ply wound at $-30°$. The reason for this change in behaviour is the presence of the outer layer of $-30°$ wind angle. Due to the large thickness of this tube, the centrifugal load within this ply is higher than that acting on the ply of $+80°$ fibre orientation. Additionally, the lower curvature in this layer provides less geometric support than is available in the ply of $+80°$ orientation. Since the material of the $+80°$ ply is also much stiffer circumferentially than the $-30°$ ply, it provides significant constraint to the radial displacement of this ply, and thereby carries a significant component of the centrifugal load arising within it. The tensile radial stress within the $+80°$ ply is therefore increased by the outwards radial load of the $-30°$ ply. The radial stress in the outer ply of $-30°$ wind angle decreases rapidly, and almost linearly, from the ply interface down to zero at the outer surface of the tube.

The through-thickness axial stress distributions of the thin and thick-walled rotating GFRP tubes, determined using both the current analytical solution and FE simulation, are presented in Fig. 4. Although centripetal acceleration results in centrifugal loads that act only in the radial orientation, axial stresses arise as a consequence of the coupled nature of the material, and the equilibrium and continuity conditions associated with the cylindrical nature of the tubes. It is clear from this figure that the analytical and FE solutions are in excellent agreement with one another in both cases, once again validating the current extension of the displacement-based analytical solution to include centrifugal forces. The axial stresses that develop through the thickness of both tubes are discontinuous across each ply interface, and are of sufficient magnitude that they cannot be neglected. The plane-stress assumption for these particular problems is clearly incorrect. The constant through-thickness axial strains, ε_x^0, which arise are roughly -975 $\mu\varepsilon$ for the thin-walled tube, and approximately -656 $\mu\varepsilon$ for the thick-walled tube. These values are large enough that the plane-strain approximation

is also invalid. The axial strain response of the thin-walled tube is larger in magnitude than that of the thick-walled tube as a direct result of the larger hoop stresses that develop within this tube, seen in Fig. 2. Since the body forces that arise under centrifugal loading act only in the radial direction, no axial force can exist at the ends of the tube. Integration of the axial stress distributions of Fig. 4 produce zero-force resultants which adhere to this requirement, but this can be expected anyway because this condition is enforced by the use of Eq. (63) when determining the required A_1^k and A_2^k constants of each layer of the GFRP tubes. The through-thickness axial stress distributions of the thin and thick-walled tubes are quite different from one another, particularly within the innermost plies wound at $+20°$ and $-45°$. The magnitude of the axial stresses are largest in the thin-walled tube, associated with the larger axial strain response of this configuration. It is interesting to note that for both the thin and thick-walled tubes, the largest axial stress develops within the plies of $-45°$ fibre orientation. This is some-

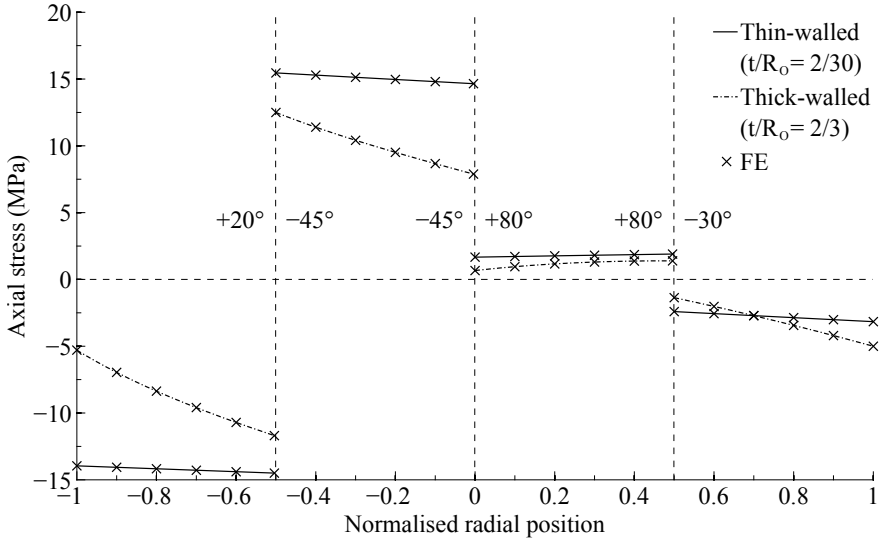

Figure 4: Axial stress distributions for thin and thick-walled 4 layer anisotropic GFRP tubes

what unexpected and, since the axial strain across the wall thickness of each tube is constant, one might expect the largest axial stress to arise within the plies of highest axial stiffness, and hence smallest wind angle, being the plies of $+20°$ fibre orientation. This unexpected behaviour is associated with the coupled nature of the axial, hoop, radial and shear stress components. For both configurations, the hoop stresses within the $-45°$ plies, seen in Fig. 2 are larger than those that develop within the plies of $+20°$ fibre orientation, and the coupling between the axial and hoop components causes the axial stresses within these plies to be slightly larger than those which develop within the $+20°$ plies. The axial stresses, however, remain highly dependant upon the axial strain response of the tubes, and since the axial stiffness of the plies wound at $+80°$ are significantly lower than any of the other plies, the stresses that arise within these layers are of lowest magnitude. An interesting result lies in the magnitude of the axial stresses

within the plies of -30° wind angle. This fibre orientation has an axial stiffness considerably larger than that of the plies of -45° wind angle. The axial stresses within the -30° plies are, however, of significantly lower magnitude. This behaviour highlights the radial dependence of the stresses. As the radial position increases, so the magnitude of the hoop stresses within an individual ply generally decreases. This is most apparent within the stress distributions of the thick-walled tube seen in Fig. 2. Since the ply of -30° wind angle lies considerably further out radially than the -45° ply, the hoop stress in this ply is substantially lower and, as a consequence of the coupled nature of the problem, this results in lower axial stresses even though the axial material stiffness is higher.

Although no torque load is applied to the ends of the GFRP tubes, the anisotropic nature of the particular wind configuration under consideration results in the formation of in-plane shear stresses under the centrifugal loading condition. These stresses, determined using the current analytical method and FE approach are presented in Fig. 5, for both the thin and thick-walled configurations. The stress distributions determined using both methods are indistinguishable from one another, validating the results of the extension to the elastic solution presented in this work. The shear stresses that develop through the wall thickness of the tube are of similar magnitude to the axial stresses that arise, which are presented in Fig. 4. Additionally, much like the axial stress solutions, since no torque load is applied at the ends, the integral of the moment of the shear stresses about the centre of the tube is zero. This is an expected result, since this condition is enforced by the use of Eq. (64) to determine the required values of the A_1^k and A_2^k constants for each layer of the tubes. It is worth noting the sense of the slopes in shear stress within each of the plies. For the plies of positive wind angle, the slope in shear stress is negative, whereas positive slopes in stress occur within the plies of negative wind angle. This is most apparent for the results of the thick-walled tube. This behaviour is quite strange, and since, by Eq. (54), the in-plane shear strain across the wall thickness of a tube increases linearly with radius, one might expect the slopes of the shear stresses within all layers to share the same sense, and for the magnitude of the shear stresses within each layer to increase with increased radial position. This does not occur, simply because the twist within the tubes is low. The constant angle of twist, γ^0, is 9.8×10^{-6} rad/mm for the thin-walled case and -21.4×10^{-6} rad/mm for the thick-walled case. The resultant shear strain distributions that exist through the wall thickness of these tubes is also low, and the shear stresses of Fig. 5 are therefore dependant almost entirely on the coupling between the normal and shear stress components. It is for this reason that the change in the slope of shear stresses with positive and negative fibre orientation occurs. With this in mind, consider the shear stress distribution of the thin-walled tube. The largest shear stress develops within the ply of $+80^\circ$ fibre orientation, with a value of close to 18 MPa, which can be related back to the very high hoop stress that develops within this ply, as seen in Fig. 2. The shear stresses that develop within the -45° ply are of similar magnitude, despite the significantly lower hoop stresses that arise within this ply. This ply, however, has the highest shear stiffness and largely counteracts the shear stresses in the $+80^\circ$ ply. This results in this ply having the largest axial stresses, as seen in Fig. 4. For the thick-walled tube, the largest shear stress, with a value of close to -12 MPa, occurs within the ply of -45° wind angle, followed by a stress of just more than 7 MPa within the ply wound

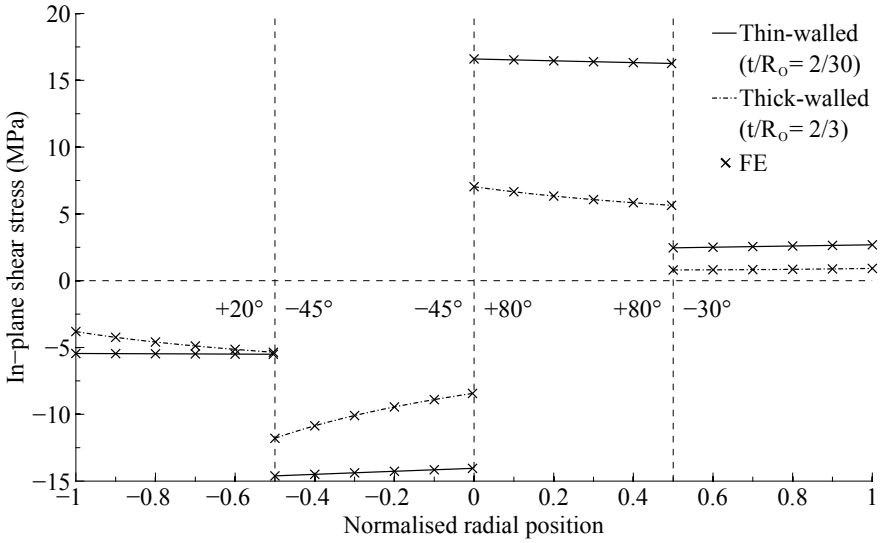

Figure 5: Shear stress distributions for thin and thin-walled 4 layer anisotropic GFRP tubes

at $+80°$. Again, these stress arise because of the coupled nature of the shear stresses to the normal stress components.

Conclusions

The displacement-based elastic solution for infinitely long, layered anisotropic tubes has been extended to include the effects of centrifugal loading. The elastic response of a tube subject to this type of loading is described by additional terms in the existing equations of the solution. This allows the behaviour of a layered anisotropic tube under combined axisymmetric loading and centrifugal load to be computed. The additional terms of the current extension have been validated by considering both thin and thick-walled GFRP tubes of arbitrary anisotropic lay-up under pure centrifugal load, and comparing the stress solutions of the analytical approach against the those obtained by FE simulation. The results of the two methods are indistinguishable. A comparison between the stress distributions of the thin and thick-walled sections has been presented, and it has been demonstrated that the stresses that arise under the centrifugal loading condition are highly dependant upon t/R_O ratio, lay-up, and stacking sequence. It is shown that for both thin and thick-walled tubes, neither the plane-stress nor the plane-strain assumptions are valid. Although no loads are directly applied in these senses, both axial stresses and in-plane shear stresses of considerable magnitude can arise as a consequence of coupling between the normal and shear components associated with the anisotropic nature of the problem. The current analytical solution is linear and is consequently only valid under conditions where the radial displacement of the tube is relatively small. The solution does not account for the change in centrifugal load with the geometric changes. Care must be taken, therefore, when considering tubes rotating

at very high angular velocities, or when the material from which the tube is composed is of relatively low modulus.

Acknowledgements

The support of the DST/NRF towards this research is hereby acknowledged. Opinions expressed and conclusions arrived at, are those of the authors and are not necessarily to be attributed to the DST/NRF.

References

[1] S.G. Lekhnitskii. *Theory of Elasticity of an Anisotropic Elastic Body*. Holden-Day, 1963.

[2] T. Chen, C. Chung, and W. Lin. A revisit of a cylindrically anisotropic tube subjected to pressuring, shearing, torsion, extension and a uniform temperature change. *International Journal of Solids and Structures*, 37(37):5143–5159, 2000.

[3] V.E. Verijenko, S. Adali, and P.Y. Tabakov. Stress distribution in continuously heterogeneous thick laminated pressure vessels. *Composite Structures*, 54(2):371–377, 2001.

[4] X.S. Sun, V.B.C. Tan, Y. Chen, L.B. Tan, R.K. Jaiman, and T.E. Tay. Stress analysis of multi-layered hollow anisotropic composite cylindrical structures using the homogenization method. *Acta Mechanica*, 225(6):1649–1672, 2014.

[5] W.A. Olson and C.W. Bert. Analysis of Residual Stresses in Bars and Tubes of Cylindrically Orthotropic Materials. *Experimental Mechanics*, 6(9):451–457, 1966.

[6] G.Z. Voyiadjis, P.D. Kiousis, and C.S. Hartley. Analysis of residual stresses in cylindrically anisotropic materials. *Experimental Mechanics*, 25(2):145–147, 1985.

[7] G.Z. Voyiadjis and C.S. Hartley. Residual-stress determination of concentric layers of cylindrically orthotropic materials. *Experimental Mechanics*, 27(3):290–297, 1987.

[8] J. Rasty, X. Le, M. Baydogan, and J.F. Cárdenas-García. Measurement of residual stresses in nuclear-grade Zircaloy-4(R) tubes - Effect of heat treatment. *Experimental Mechanics*, 47(2):185–199, 2007.

[9] A.N. Stroh. Dislocations and Cracks in Anisotropic Elasticity. *Philosophical Magazine*, 3(30):625–646, 1958.

[10] T.C.T. Ting. Pressuring, Shearing, Torsion and Extension of a Circular Tube or Bar of Cylindrically Anisotropic Material. *Proceedings of the Royal Society of London A: Mathematical, Physical and Engineering Sciences*, 452(1954):2397–2421, 1996.

[11] T.C.T. Ting. New solutions to pressuring, shearing, torsion and extension of a cylindrically anisotropic elastic circular tube or bar. *Proceedings of the Royal Society of London A: Mathematical, Physical and Engineering Sciences*, 455(1989):3527–3542, 1999.

[12] L.F. Ma, Y.H. Chen, and S.Y. Zhang. On the explicit formulations of circular tube, bar and shell of cylindrically piezoelectric material under pressuring loading. *International Journal of Engineering Science*, 39(4):369–385, 2001.

[13] J.Q. Tarn and Y.M. Wang. Laminated composite tubes under extension, torsion, bending, shearing and pressuring: a state space approach. *International Journal of Solids and Structures*, 38(50–51):9053–9075, 2001.

[14] X. Wang and Z. Zhong. A circular tube or bar of cylindrically anisotropic magnetoelectroelastic material under pressuring loading. *International Journal of Engineering Science*, 41(18):2143–2159, 2003.

[15] R.E. Sherrer. Filament-Wound Cylinders with Axial-Symmetric Loads. *Journal of Composite Materials*, 1(4):344–355, 1967.

[16] E. Reissner and W.T. Tsai. Pure bending, Stretching, and Twisting of Anisotropic Cylindrical Shells. *Journal of Applied Mechanics*, 39(1):148–154, 1972.

[17] J.F. Wilson and G. Orgill. Linear Analysis of Uniformly Stressed, Orthotropic Cylindrical Shells. *Journal of Applied Mechanics*, 53(2):249–256, 1986.

[18] G. Orgill and J.F. Wilson. Finite Deformations of Nonlinear, Orthotropic Cylindrical Shells. *Journal of Applied Mechanics*, 53(2):257–265, 1986.

[19] L.P. Kollár, J.M. Patterson, and G.S. Springer. Composite cylinders subjected to hygrothermal and mechanical loads. *International Journal of Solids and Structures*, 29(12):1519–1534, 1992.

[20] L.P. Kollár and G.S. Springer. Stress analysis of anisotropic laminated cylinders and cylindrical segments. *International Journal of Solids and Structures*, 29(12):1499–1517, 1992.

[21] C.Q. Rousseau, M.W. Hyer, and S.S. Tompkins. Stresses and Deformations in Angle Ply Composite Tubes. *CCMS-87-04 Report (VPI-E-87-3), Virginia Polytechnic Inst. and State Univ., Blacksberg*, 1987.

[22] M.S. Derstine, M.J. Pindera, and D.E. Bowles. Combined mechanical loading of composite tubes. *CCMS-88-11 Report (VPI-E-88-18), Virginia Polytechnic Inst. and State Univ., Blacksberg*, 1988.

[23] C.T. Herakovich. *Mechanics of Fibrous Composites*. John Wiley & Sons, Inc., 1998.

[24] M. Xia, H. Takayanagi, and K. Kemmochi. Analysis of multi-layered filament-wound composite pipes under internal pressure. *Composite Structures*, 53(4):483–491, 2001.

[25] H. Bakaiyan, H. Hosseini, and E. Ameri. Analysis of multi-layered filament-wound composite pipes under combined internal pressure and thermomechanical loading with thermal variations. *Composite Structures*, 88(4):532–541, 2009.

[26] M. Tervonen and A. Pramila. Stresses in a hollow rotating cylindrically orthotropic tube. *Mechanics of Composite Materials*, 32(6):577–581, 1996.

[27] A.M. El-Naggar, A.M. Abd-Alla, and S.M. Ahmed. On the rotation of a non-homogeneous composite infinite cylinder of orthotropic material. *Applied Mathematics and Computation*, 69(2–3):147–157, 1995.

[28] A. M. El-Naggar, A. M. Abd-Alla, M. A. Fahmy, and S. M. Ahmed. Thermal stresses in a rotating non-homogeneous orthotropic hollow cylinder. *Heat and Mass Transfer*, 39(1):41–46, 2002.

[29] A.M. Abd-Alla, A.N. Abd-Alla, and N.A. Zeidan. Thermal stresses in a nonhomogeneous orthotropic elastic multilayered cylinder. *Journal of Thermal Stresses*, 23(5):413–428, 2000.

[30] A.M. Abd-Alla and S.R. Mahmoud. Magneto-thermoelastic problem in rotating non-homogeneous orthotropic hollow cylinder under the hyperbolic heat conduction model. *Meccanica*, 45(4):451–462, 2010.

[31] H.L. Dai, T. Dai, and H.Y. Zheng. Stresses distributions in a rotating functionally graded piezoelectric hollow cylinder. *Meccanica*, 47(2):423–436, 2012.

[32] P.M. Wild and G.W. Vickers. Analysis of filament-wound cylindrical shells under combined centrifugal, pressure and axial loading. *Composites Part A: Applied Science and Manufacturing*, 28(1):47–55, 1997.

[33] A.M. Abd-All, A.N. Abd-alla, and N.A. Zeidan. Transient thermal stresses in a rotation non-homogeneous cylindrically orthotropic composite tubes. *Applied Mathematics and Computation*, 105(2–3):253–269, 1999.

[34] L. Parnas and N. Katırcı. Design of fiber-reinforced composite pressure vessels under various loading conditions. *Composite Structures*, 58(1):83–95, 2002.

[35] J.Q. Tarn. Exact solutions for functionally graded anisotropic cylinders subjected to thermal and mechanical loads. *International Journal of Solids and Structures*, 38(46):8189–8206, 2001.

[36] E. J. Hearn. *Mechanics of Materials 2*. Butterworth-Heinemann, Oxford, Third edition, 1997.

[37] *Linear Static, Normal Modes, and Buckling Analysis Using MSC.Nastran and MSC.Patran*. NAS 120 Course Notes. MSC. Software Corporation, 2006.